RADIOTRONICS

IN THIS ISSUE

9

OPTICAL MASERS

By DR. J. P. WITTKE

RCA Laboratories, Princeton, N.J.

Ever since the first demonstration of microwave amplification by the use of stimulated emission, there has been speculation as to whether or not the maser concept could be successfully applied in the infrared and visible portion of the electromagnetic spectrum. As early as 1956, R. H. Dicke proposed[1] a means of making an ammonia-beam maser in the infrared, using the rotational energy levels of the ammonia molecule. In the past few years, people have been optimistic about extending maser techniques into the visible portion of the spectrum. The basic principles underlying all masers — microwave, infrared, and visible—are the same,[2] but the problems that arise in achieving practical embodiments of the maser concept differ radically as one goes from the microwave frequency region (10^9 to 10^{11} cps) to the visible range (frequencies of 10^{14} to 10^{15} cps). These concepts are discussed here, as in the current state of the art and some possible applications.

Two examples will illustrate the changes required in increasing the frequency by four orders of magnitude—i.e., in going from the microwave to the visible range of the spectrum.

One is the *resonant structure* required to concentrate the electromagnetic field. At microwave frequencies, wavelengths are of the order of a centimeter, and cavities can be built that are one, or at most a few, half-wavelengths long. The modes of the resonator are generally well resolved, and it is no problem to couple the emissive material to the desired cavity mode. Optical wavelengths, on the other hand, are so small that it is impossible to build useful structures a few wavelengths across, and much larger structures must be employed. These large structures can be expected to sustain many modes very close together in frequency and of comparable Q. Moding may thus be a serious problem in optical masers, whereas it is not of concern at microwave frequencies.

A second example of a new problem arising at optical frequencies is that due to *spontaneous emission*. Atoms in excited states tend to return to their lowest energy (ground) state by the emission of radiation. This process has two harmful effects in a maser: it provides an alternative method of de-excitation, reducing the size of the population excess in the upper state; and the spontaneously radiated energy, being incoherent with the signal wave field, is an additional source of noise in a maser amplifier or oscillator.

Neglecting possible coherence effects in spontaneous emission, a system having N_2 atoms in excited states will lose energy by *spontaneous* emission at a rate (P_{sp}):

$$P_{sp} = \frac{4\omega^4 \mu^2 N_2}{3c^3} \qquad (1)$$

Where: ω is the circular frequency of the radiation, μ is the dipole moment associated with the transition between the ground and excited states, and c is the velocity of light.

By comparison, the power (P_{st}) radiated by a system with ΔN atoms in the "excess" upper state population due to *stimulated* emission is:

$$P_{st} = \frac{h\omega}{\Delta\omega}\left(\frac{\mu E}{h}\right)^2 \Delta N \qquad (2)$$

where $h = h/2\pi$, h is Planck's constant (6.624×10^{-34} joule-sec), E is the strength of the electric vector in the electromagnetic field inducing the transistor, and $\Delta\nu = \Delta\omega/2\pi$ is the spectral width associated with the response of the atom to the field ($\omega/\Delta\omega$ is an effective atomic Q for the transition).
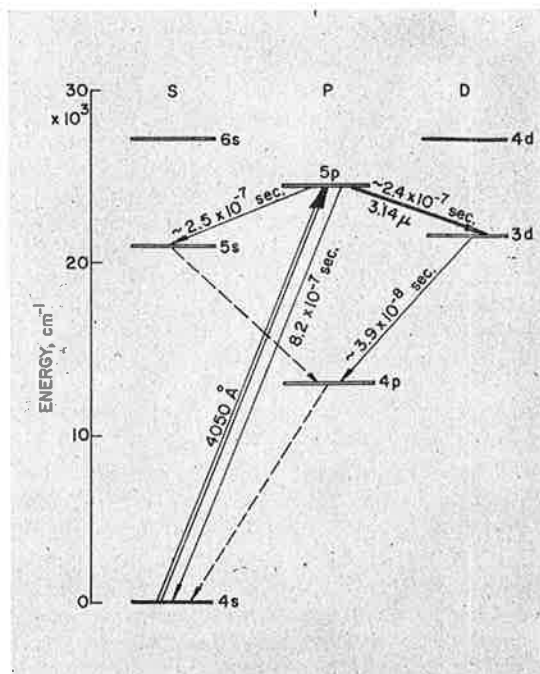

Fig. 1—Energy levels associated with the excitation of the valence electron of a potassium atom in the vapour.

The important point to note from equations 1 and 2 is that the relative importance of spontaneous emission varies as the cube of the frequency. Thus, it is of the order of 10^{12} times as important at optical as at microwave frequencies.

Another difference between optical and microwave masers is in the nature of the internal energy states that are utilized. Microwave frequencies correspond to energies of the order of 10^{-4} electron volts; internal energy states separated by such energies can be found associated with orientational energies of intrinsic electronic magnetic moments in laboratory-scale magnetic fields (a few thousand gauss). The atoms are thus acted on by microwave *magnetic* fields to produce the desired transitions. Transitions corresponding to optical radiation, on the other hand, have energies of the order of an electron volt. These much more energetic transitions are associated with changes in the state of motion of electrons in

atoms and are generally brought about by the action of the *electrical* component of the radiation field.

Excitation Methods

Several methods have been proposed to bring about the required emissive inverted population distribution in an optical maser. As mentioned, Dicke has shown that molecular beam maser techniques can be extended into the infrared. Others have proposed optical masers using three or more energy levels.

In one such scheme, proposed by Schawlow and Townes,[3] the energy levels are those associated with the excitation of the valance electron of an alkali metal atom in the vapour (Fig. 1). Here, radiation at a higher frequency than that of the desired signal excites atoms from the ground state to some excited state, from whence they decay to states of lower excitation, eventually returning to the ground state by a series of one or more spontaneous emission processes.
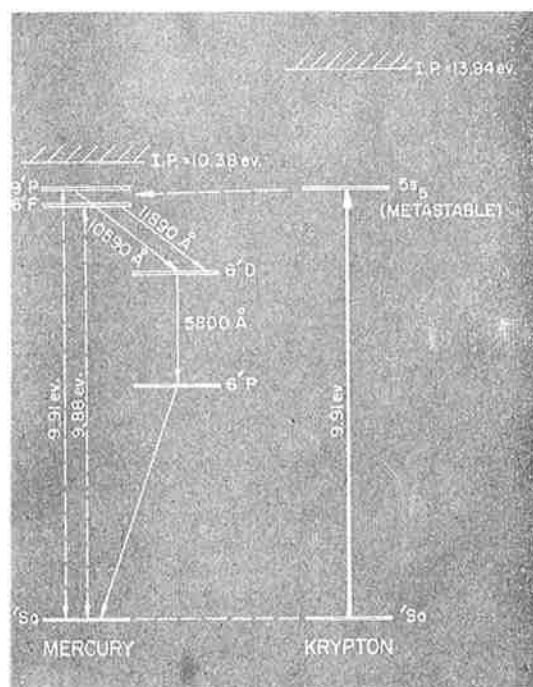

Fig. 2—A method of indirect electron collision excitation of a maser gas (mercury vapour) by mixing it with a more dense auxiliary gas (krypton) in an rf discharge.

In general, several alternate decay modes are available to an atom in an excited state; for example, referring to Fig. 1, a potassium atom excited to its $5p$ state can decay to the $5s$, $3d$, or $4s$ states. Various different decay rates are associated with these competing, alternative processes. In the case illustrated, an atom excited to the $5p$
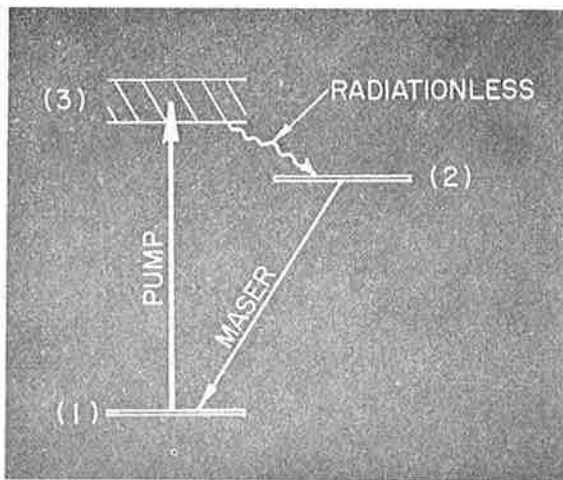
Fig. 3—Energy-level scheme utilising a solid (e.g., ruby) instead of a gas.

state has roughly equal probability of decaying to the 5s and 3d states, while it is considerably less likely that it will decay directly to the ground state. (Only about one atom in eight returns directly to the ground state.) Atoms which decay to the 3d state are rapidly removed from this state by decay to the 4p state. Thus, when potassium atoms are optically excited to the 5p state, spontaneous decay processes tend to build up a population distribution such that there are more atoms in the (relatively long-lived) 5p state than in the (quickly decaying) 3d state. Schawlow and Townes therefore suggested that this optical pumping process might be used to set up an emissive condition in the vapour for the 3.14-micron infrared radiation coupling this pair of states.

A basic difficulty of this method of obtaining an emissive state is associated with the spectral sharpness, or narrow bandwidth, associated with these optical vapour-phase transitions. Because the spectral lines are so sharp, it is very difficult to get an excited lamp that can produce much pumping radiation in the narrow band of frequencies necessary to excite an atom to the desired state.

Because of this, alternate methods of excitation of gas atoms have been proposed. One, by Sanders,[4] utilizes electron bombardment in a gas discharge. Here basically the same processes would occur, except the excitation would be by transfer of part of the kinetic energy of the hot electrons in the discharge to the gas atoms connected with the maser action. There is one additional complication in this scheme, in that presumably the electrons would tend to excite atoms into the lower, as well as the upper, maser level.

To obtain a greater population excess in the upper of a pair of energy states than one might expect from either of the aforementioned ways of exciting a gas, Javan[5] and others have suggested yet another scheme. This also involves the use of electron-collision excitation. However, now the maser gas is not excited directly. The maser gas is mixed with a different gas of much higher pressure that has the following properties: it has a metastable state of long lifetime that requires the same amount of excitation energy as an excited state of the maser gas. A possible combination is shown in Fig. 2, where mercury vapour is the maser material and krypton is the more dense auxiliary gas. The electrons in the gas discharge excite the metastable $5s_5$ level of krypton. Because of the long lifetime of this state, an appreciable number of atoms are built up in this state. There is therefore a good chance that one of the mercury maser atoms will collide with an excited krypton atom, and since the 9^1P and 6^1F states of mercury have nearly the same excitation energy as the krypton atom, there is a high probability that in a collision there will be a resonant transfer of energy between the atoms. As a result of such a collision, the krypton atom is de-excited, and the mercury atom is left in either the 9^1P or 6^1F level. Maser action may then take place between one of these states and a lower, unpumped level such as the 6^1D state shown.

There is another way in which the difficulty associated with narrow spectral lines in the optically pumped vapour scheme can be avoided. If instead of a gas, a solid is used, it is possible to find fluorescent centres that have an energy-level structure such as shown in Fig. 3. Here state 1 is the ground state, state 2 is a relatively long-lived state connected to the ground state by
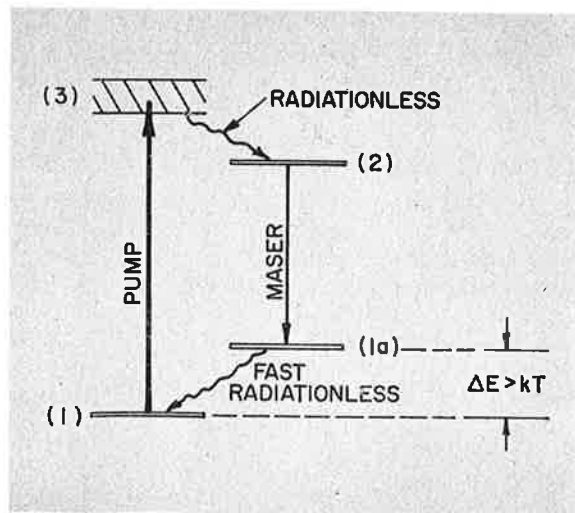

Fig. 4—Energy-level scheme utilising a solid with an additional short-lived energy level (1a).

a sharp optical transition, and state *3* is a broad state into which atoms can be excited by radiation at any frequency in a broad absorption band. In certain solids, such as ruby (chromium-doped aluminium oxide), this energy scheme can be found; moreover, a chromium ion excited to the broad level *3* decays rapidly (and in a *radiation-less* fashion) to state *2*. Thus radiation in a broad band excites atoms from the ground state to state *2* via the short-lived state *3*. If the excitation rate is high enough, this process can depopulate state *1* and populate state *2* sufficiently that maser action can be obtained between states *2* and *1*.

Because in this scheme state *1* is the ground state and hence initially contains all the atoms, it requires a very intense excited lamp to obtain the necessary population inversion. However, if the solid has an additional short-lived energy level, sufficiently far above the ground state that it remains essentially depopulated, the situation is considerably improved. This is illustrated in Fig. 4. Here, a new level (state *1a*) lies $\Delta E > kT$ above the ground state, kT being the average thermal excitation energy at temperature T. Now maser action can occur between states *2* and *1a* without the ground state being heavily depopulated, since both states participating in the maser action are normally depopulated. A sufficiently rapid decay from *1a* to *1* is, of course, required. Several solids meet these requirements, such as calcium fluoride doped with uranium, and calcium fluoride doped with samarium.

Optical Maser Characteristics

If an electromagnetic wave propagates through an emissive medium, the amplitude of the wave will grow exponentially with distance until saturation effects make the system non-linear. Such an emissive medium thus acts as a travelling wave amplifier, with a gain G given by:

$$G = \exp(\alpha L) \qquad (3)$$

where: L is the length of the amplifier, and α is the gain coefficient. This is related to the parameters of the maser material by:

$$\alpha = \frac{4\omega\mu^2 \Delta N}{hc\Delta v} \qquad (4)$$

Instead of using dipole moments μ, spectroscopists frequently express the strength of optical transitions in terms of oscillator strengths f. These are related to the dipole moments by:

$$f = \left(\frac{2m}{he^2}\right)\omega\mu^2 \qquad (5)$$

where: m and e are the electronic mass and charge, respectively. In terms of oscillator strengths:

$$\alpha = \left(\frac{2e^2}{mc}\right)\left(\frac{f\Delta N}{\Delta v}\right)$$
$$= 1.68 \times 10^{-2}\left(\frac{f\Delta N}{\Delta v}\right) \qquad (6)$$

For narrow optical transitions in solids, typical values for f and Δv are $f \approx 10^{-6}$, $\Delta v \approx 10^{10}$ cps. This gives $a \approx 10^{-18}\Delta N$. Since ΔN is not apt to exceed 10^{+18}, (and even this is quite an optimistic value), the need for a field-concentrating resonant structure to increase the effective optical path in any device of practical size is readily seen.

A high Q resonator that appears quite suitable for use in an optical maser is a pair of Fabry-Perot plates.[1,3] Such a resonator is illustrated in Fig. 5. Radiation, essentially in the form of a (limited-extent) plane wave can bounce back and forth between the mirrored surfaces for many times, enhancing its interaction with the maser material. One of the plates is slightly transmitting, permitting a small amount of the energy incident on this end to be coupled out into a useful beam.

The exact behaviour of an oscillator formed by making the silvering of the Fabry-Perot plates dense enough to supply the required positive feedback is very complex and has not yet been treated in detail. Schawlow and Townes give plausible arguments showing that one might expect a spectral purity of the emitted radiation of the order of:

$$\delta v = \frac{4\pi h\omega (\Delta v)^2}{P} \qquad (7)$$

where: δv is the width of the oscillator spectrum, and P is the emitted power from the oscillator. Inserting reasonable values into this equation, it appears that spectral widths of a few cps might be expected. Since optical frequencies are in the range 10^{14} to 10^{15} cps, this corresponds to fantastic spectral purity and, if achieved, would permit a variety of applications (some of which will be discussed later).
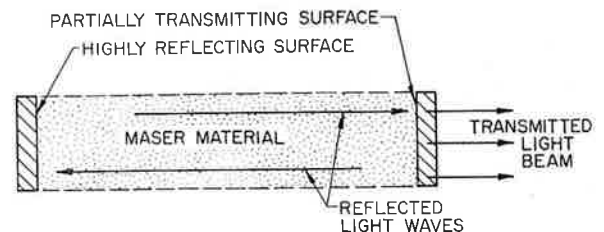
Fig. 5—A high-Q resonator for an optical maser, a pair of Fabry-Perot plates.

In addition to this extreme monochromaticity, which corresponds to a coherence length of the order of 50,000 miles, a maser oscillating in a single planewave Fabry-Perot mode would have an output beam limited in directivity by diffraction effects at the output Fabry-Perot plate. For a resonator diameter of the order of an inch and a wavelength of 7500 angstroms, diffraction effects would limit the beam to one diverging at an angle of 3×10^{-5} radians. This high degree of spatial coherence in the wave front corresponds to an illuminated spot diameter of about one yard at a distance from the maser of twenty miles.

Present State of the Art

With a field that is as rapidly moving as this, it is dangerous to assume that any description of the state of the art will not be outdated by the time of publication. Nevertheless, an attempt will be made.

Work on an optically-excited alkali vapour maser is under way at Columbia University. Various electron-excitation schemes are being studied at a number of places, notably at the Bell Telephone Laboratories and at the Technical Research Group. The workers at Bell have recently been successful in operating an electron-excited gaseous optical maser.[6]

With optically-excited solids, Maiman[7] (at Hughes) reported maser action in ruby during mid-1960, and since then several groups, including one at RCA Laboratories, have repeated and extended Maiman's work with ruby. In many of the experiments with ruby, a ruby rod polished to have plane parallel ends, which are silvered to act as Fabry-Perot mirrors, was excited by being placed inside a helical photoflash lamp. The brilliant flash of the lamp inverted the populations of the ground and long-lived excited states in the ruby, and for a few hundred microseconds (while the flash tube was on), coherent stimulated emission was observed from one partially transparent end of the ruby rod. Other flash lamp-sample configurations have also been used successfully.

Because of the disadvantage of using the ground state as the lower maser state, considerable work is under way at many locations, including RCA Laboratories, to discover other maser materials without this disadvantage. Workers elsewhere have recently reported[8,9] two such materials.

Outstanding Problems

Although the past few months have produced striking advances in the optical maser art, many problems remain. Some of these are illustrated by the ruby masers that have been operated. In ruby, the workers at Bell find[10] that the maser oscillation is not continuous during the exciting pulse, but occurs in short, quasi-random bursts of about one-microsecond duration. The cause of this behaviour is not known, nor is its cure. Moreover, although peak maser powers of the order of ten kilowatts have been reported, the corresponding spectral purity given by equation 7 has not been attained, or even closely approached. Equation 7 would give a linewidth of well under one cps. However, because the radiation occurs in microsecond-long pulses, one would expect a linewidth of the order of 10^6 cps. Instead, however, spectral widths of the order of 6×10^8 are the narrowest that have been observed. Also, instead of a diffraction-limited beam angle, angular divergences some twenty times as large are observed. While plausible explanations can be given for some of these apparent discrepancies, it has not yet been shown experimentally that the postulated causes of non-optimal behaviour are in fact the actual ones.

Thus far, only pulsed operation of solid state optical masers has been reported, although the pulse lengths have been extended to a point where continuous operation requires but little improvement. Of the solid state masers, two exhibit the "short-burst" type of operation, while one (Sm^{2+} in CaF_2) shows no evidence of this rapid uncontrollable amplitude modulation. It is not yet known why the various materials do or do not show the "burst" type of oscillation modulation. (The gaseous maser that has been operated is also free from this type of modulation.)

Possible Applications

The applications that one can foresee for optical masers depend primarily on the coherent nature of the interaction. This is responsible for both the spatial and temporal coherence of the radiation pattern from a maser oscillator, and the virtues of such devices are closely tied to these properties. For example, because of the high directivity, corresponding to an antenna gain of the order of 10^{10}, optical masers open up the possibility of optical point-to-point communications systems that may be extremely important in space communications. Moreover, the narrow beam permits optical radars of much higher directional resolution than microwave radars. The monochromaticity of an optical maser offers to promise that heterodyne information-handling techniques may be extended to visible frequencies, where the extremely high frequencies are associated with bandwidths many orders greater than available at lower frequencies. As an indication of possibilities in this line, "optical waveguides" that could in principle transmit all the telephone channels between two large cities in one small pipe are under consideration. These are, of course, far from realization in a system at present.

RECTIFIER CHARACTERISTICS
CALCULATOR

The two-page chart which follows on the next two pages is intended to assist in calculating and setting up seven of the more popular configurations of rectifier circuit, with special emphasis on the use of silicon diode rectifiers. The chart contains six main columns, which are arranged as follows:

Column 1 shows the basic circuit arrangement, and the points at which the rms input voltage and the average output voltage are measured. Note that the rectifier forward voltage, rectifier reverse current and source reactance are all taken as zero for the purposes of the chart. It must therefore be remembered that items such as a rectifier surge protection resistor are not included in the calculations. It is however a simple matter to make provision for variations of this kind.

Column 2 deals with the dc output voltage, which is more often than not the starting point of the exercise. It is sub-divided into four items, which are respectively the average dc output voltage, the peak output voltage, the output waveform related to one cycle of the supply voltage, and the ripple percentage which may be expected. There is of course no filtering applied at this stage.

The third column deals with the rms ac input voltage, which in this case means the appropriately labelled voltage in the sample circuit given in the first column. The voltages are quoted for resistive or inductive load conditions.

Column number 4 states the average total dc output current or load current. Here, again, like the average dc output voltage, this is generally one of the given facts at the start of the calculation.

The fifth column is a very important one, as it deals with the current rating per rectifier cell or unit. This refers to the individual units shown in the typical circuit of column one. The current ratings, like the voltage ratings, may be adjusted if required for cases where two or more units are used in series or parallel to obtain a greater voltage or current rating than can be catered for by one unit only.

The current waveform is shown in relation to one cycle of the supply voltage (or current), together with the average current per rectifier

unit in relation to the total dc output current of the circuit. Figures are also given for the rms current rating, peak current rating, and the ratio of peak-to-average current for each rectifier unit, all related to the total dc output current of the circuit; these figures are given in two sets, one for a resistive load and the other for an inductive load.

Finally, column 6 gives us the peak inverse voltage per cell or rectifier unit, in terms of both the average dc output voltage of the circuit and of the rms input voltage specified in the circuit.

To show how this chart may be used, two worked examples will be quoted.
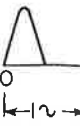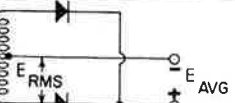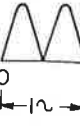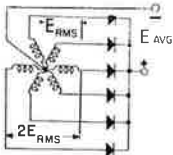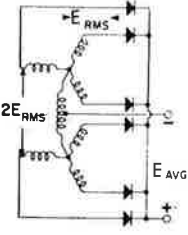
Typical Solution No. 1
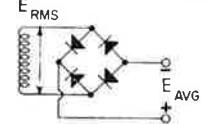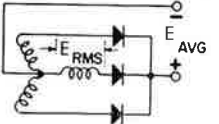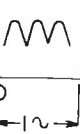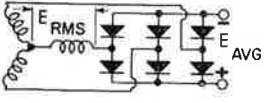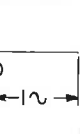
In this case it is assumed that the requirement is a single-phase, half-wave circuit with resistive load. The required dc output voltage (E_{avg}) is 150 volts, and the required dc output (load) current (I_{avg}) is 19 amperes.
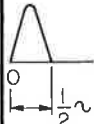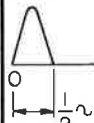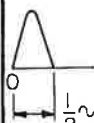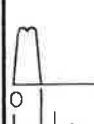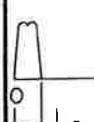
First the rms input voltage E_{rms} is found from column 3, at 2.22 times E, which is 333 volts. For the current ratings of the rectifier we go to column 5, with the average current at 19 amperes, the rms current 1.57 times that at 30 amperes, and the peak current 3.14 times the average value at 60 amperes. Finally, from column 6 we find that the peak reverse voltage on the rectifier unit is 3.14 times the average dc output voltage of the circuit, at 472 volts. Alternatively, we can obtain the same figure from a calculation of 1.41 times the rms input voltage E_{rms}.

Typical Solution No. 2

In this case we require a single-phase, full-wave bridge circuit to supply a resistive load. The given data are that the ac input voltage E_{rms} is 30 volts, and that the dc load current (total) is 65 amperes; this is the quantity I_{avg}.

The factors given in column 5 allow us to calculate the average current per rectifier unit at 32.5 amperes, the rms current per rectifier unit at 51 amperes, and the peak current per rectifier unit at 102 amperes. From columns 2 and 3 the dc output voltage can then be determined at 1.11 times E_{rms}, which is 27 volts. The peak reverse voltage per rectifier element is found through column 6 to be 42 volts.

(1) CIRCUIT	(2) DC OUTPUT VOLTAGE				(3) AC INPUT VOLTAGE (RMS)	
(Rectifier forward voltage, reverse current, and source reactance = zero)	Average	Peak	Wave-form	Per cent Ripple	PHASE	LINE-TO-LINE
					For Resistive or Inductive Load	
Single-Phase Half-Wave	E_{AVG}	$3.14E_{AVG}$		121	E_{RMS} $2.22E_{AVG}$	
Single-Phase Full-Wave	E_{AVG}	$1.57E_{AVG}$		48	E_{RMS} $1.11E_{AVG}$ (To center tap)	$2E_{RMS}$ $2.22E_{AVG}$
Single-Phase Full-Wave Bridge	E_{AVG}	$1.57E_{AVG}$		48	E_{RMS} $1.11E_{AVG}$	E_{RMS} $1.11E_{AVG}$
Three-Phase Y Half-Wave	E_{AVG}	$1.21E_{AVG}$		18.3	E_{RMS} $0.855E_{AVG}$ (To neutral)	$1.73E_{RMS}$ $1.48E_{AVG}$
Three-Phase Y Full-Wave Bridge	E_{AVG}	$1.05E_{AVG}$		4.3	E_{RMS} $0.428E_{AVG}$ (To neutral)	$1.73E_{RMS}$ $0.74E_{AVG}$
Six-Phase Star (Three-Phase Diametric)	E_{AVG}	$1.05E_{AVG}$		4.3	E_{RMS} $0.74E_{AVG}$ (To neutral)	$2E_{RMS}$ $1.48E_{AVG}$ No load
Three-Phase Double Y and Interphase Transformer	E_{AVG}	$1.05E_{AVG}$		4.3	E_{RMS} $0.855E_{AVG}$ (To neutral)	$2E_{RMS}$ $1.71E_{AVG}$ No load

(4) TOTAL DC OUTPUT (LOAD) CURRENT	Wave-form	(5) CURRENT RATING PER RECTIFIER CELL							(6) PRV PEAK REVERSE VOLTS PER CELL
		Aver-age	For Resistive Load			For Inductive Load or High-Inductance Choke-Input Filter			
			RMS	PEAK	RATIO: PK/AV	RMS	PEAK	RATIO: PK/AV	
I_{AVG}		I_{AVG}	$1.57I_{AVG}$	$3.14I_{AVG}$	3.14	-	-	-	$3.14E_{AVG}$ $1.41E_{RMS}$
I_{AVG}		$0.5I_{AVG}$	$0.785I_{AVG}$	$1.57I_{AVG}$	3.14	$0.707I_{AVG}$	$1.00I_{AVG}$	2.00	$3.14E_{AVG}$ $2.82E_{RMS}$
I_{AVG}		$0.5I_{AVG}$	$0.785I_{AVG}$	$1.57I_{AVG}$	3.14	$0.707I_{AVG}$	$1.00I_{AVG}$	2.00	$1.57E_{AVG}$ $1.41E_{RMS}$
I_{AVG}		$0.333I_{AVG}$	$0.587I_{AVG}$	$1.21I_{AVG}$	3.63	$0.578I_{AVG}$	$1.00I_{AVG}$	3.00	$2.09E_{AVG}$ $2.45E_{RMS}$
I_{AVG}		$0.333I_{AVG}$	$0.579I_{AVG}$	$1.05I_{AVG}$	3.15	$0.578I_{AVG}$	$1.00I_{AVG}$	3.00	$1.05E_{AVG}$ $2.45E_{RMS}$
I_{AVG}		$0.167I_{AVG}$	$0.409I_{AVG}$	$1.05I_{AVG}$	6.30	$0.408I_{AVG}$	$1.00I_{AVG}$	6.00	$2.09E_{AVG}$ $2.83E_{RMS}$
I_{AVG}		$0.167I_{AVG}$	$0.293I_{AVG}$	$0.525I_{AVG}$	3.15	$0.289I_{AVG}$	$0.50I_{AVG}$	3.00	$2.09E_{AVG}$ $2.45E_{RMS}$

A Series on Tunnel Diodes

2: CHARACTERISTICS

Because of the inherent simplicity of tunnel diodes, the number of electrical characteristics of interest to circuit designers is relatively small in comparison to those for electron tubes or transistors. The essential **static characteristics** are indicated in Fig. 10, which shows the current-voltage characteristic curve for a tunnel diode. The **peak-point forward current** I_P is the value of current at which the slope of the current-voltage characteristic changes from positive to negative as the forward voltage is increased. For a given semiconductor, I_P depends primarily on the resistivity of the crystal and the junction area of the device, and can be closely controlled during fabrication to within a few per cent of the desired value. Tunnel diodes have been made with peak currents ranging from several microamperes to several hundred amperes. The actual value used is determined primarily by the application, as shown in Table 1.

The **valley-point current** I_V is the current at which the slope of the current-voltage characteristic changes from negative to positive as the forward voltage is further increased. An important relationship between peak current and valley current is the **peak-to-valley current** ratio $I_P:I_V$. This parameter determines the current swing of the device, and is particularly critical for computer-switching applications. This ratio is typically ten to one for germanium tunnel diodes, and twenty to one for gallium arsenide tunnel diodes.

The **peak voltage** V_P and the **valley voltage** V_V are the voltages at which the peak current and the valley current, respectively, occur. These voltage parameters are determined primarily by the type of semiconductor material used in the tunnel diode. (For high-current diodes, the peak voltage can also be substantially affected by the voltage drop across the series resistance of the diode.)

Voltages in the forward region greater than the valley voltage are designated by the symbol V_F. The forward voltage for which the current is equal to the peak current value is called the **projected peak voltage** V_{PP}. The symbol V_F' designates the forward voltage at which the current is equal to the maximum specified peak current, i.e., the upper tolerance limit on the rated peak current value.

The **dynamic** (or small signal) **characteristics** of tunnel diodes are defined with respect to the tunnel-diode equivalent circuit shown in Fig. 11. The most important of the dynamic characteristics is the **junction resistance** R_j of the tun-
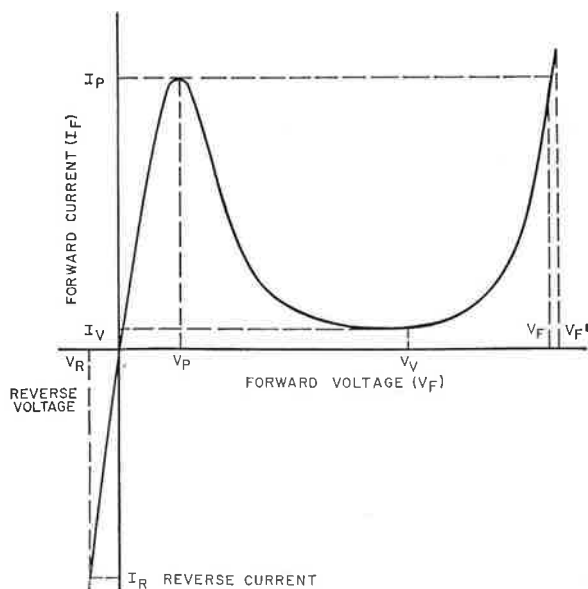

Fig. 10—Static current-voltage characteristic of a tunnel diode.

APPLICATION	PEAK CURRENT RANGE
Tunnel Rectifier	0.1 to 1 ma
Amplifier	0.5 to 2 ma
Computor Switching	2 to 50 ma
Oscillater	5 ma to 1 a
DC-to-AC Converter	above 1 a
High-current Switch	above 1 a

Table 1—Typical applications with probable peak current ranges.

nel-diode, which is determined from two measured parameters, as follows:

$$R_j = \frac{dV}{dI} - R_s \tag{1}$$

where dV/dI equals the inverse slope of the current-voltage curve and R_s equals the series resistance of the diode.

The current-voltage characteristic has an inflection point in the negative-resistance region. At that point, the magnitude of the negative resistance is a minimum and is inversely proportional to the diode peak current, as shown by

$$R_{min} = \left| R_j \right| min \cong \frac{V_k}{I_p} \tag{2}$$

where V_k is a voltage which is characteristic of the semiconductor material. The peak current is the product of tunnel-current density at the peak point J_p and the junction area A_j. The tunnel-current density is a very sensitive function of material properties (e.g., impurity concentration or crystal resistivity) and fabrication techniques (e.g., alloying time and temperature). As a result, J_p is very difficult to control during fabrication. The value of I_P (or R_{min}) must be adjusted by individual etching of each diode to its final junction area. The junction capacitance is not nearly so sensitive to material properties or fabrication techniques, but it is directly proportional to junction area. As a result, the etching process can be used to provide very tight tolerances on peak current, but the junction capacitance is not controlled so closely.

The series resistance can be considered as the resistance of the semiconductor wafer. In a well fabricated diode, the value of the ratio $R_s : R_{min}$ is often less than 0.05; however, it is difficult to
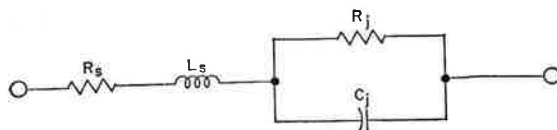

Fig. 11—Small-signal tunnel diode equivalent circuit.

maintain this ratio in the fabrication of high-frequency diodes.

The **series inductance** L_s is a property of the diode case (particularly the lead connecting the upper electrode of the diode to the case), and is influenced by the circuit in which the diode is used. The diode **junction capacitance** C_j is the small-signal capacitance associated with the p-n junction alone at a specified bias and frequency. Usually C_j is specified at the valley voltage; at this voltage, C_j is relatively insensitive to voltage and frequency. Also, the high dynamic resistance R_j in the valley region simplifies the problems of measuring C_j. (This measurement is discussed further in the chapter on Measuring Circuits.)

A small-signal analysis of the tunnel-diode equivalent circuit determines several parameters which are useful in the selection of tunnel diodes for different applications. The frequency limitations of the tunnel-diode junction alone are determined by the diode capacitance and R_{min}. This frequency capability can be described in terms of a **figure of merit** f_c which is given by

$$f_c = \frac{1}{2\pi R_{min} C_j} \tag{3}$$

The figure of merit has two very useful interpretations for negligible series resistance; it is the maximum value of the diode **gain-bandwidth** product for linear circuits, and its reciprocal determines the minimum diode **switching time** when the unit is used as a logic element.

The combination of Eqs. (2) and (3) results in the relationship:

$$f_c = \left(\frac{1}{2\pi V_k} \right) \left(\frac{I_P}{C_j} \right) \tag{4}$$

where the first term is a constant for a given semiconductor material. The second term (I_P/C_j) is, therefore, a direct measure of the diode speed capability. This parameter is frequently referred to as the diode **speed factor** or **speed index,** and is usually expressed in units of milliamperes per picofarad.

The frequency f_c should not be confused with the **resistive cutoff** frequency f_{ro} which represents the frequency at which the diode no longer exhibits negative resistance for a specified bias. When the bias is adjusted so that f_{ro} is a maximum, its value is given by

$$f_{ro} \, max = \frac{1}{2\pi R_{min} C_j} \sqrt{\frac{R_{min}}{R_s} - 1} \tag{5}$$

provided that R_{min} is greater than or equal to $2 R_s$. If R_{min} is less than $2 R_s$, then the bias must be adjusted so that the absolute value of R_j is equal to $2 R_s$ to obtain the maximum oscillating frequency.

Another quantity of interest in some applications (particularly amplifiers and oscillators) is the **self-resonant frequency** f_{xo} which is given by

$$f_{xo} = \frac{1}{2\pi R_j C_j} \sqrt{\frac{R_j{}^2 C_j}{L_s} - 1} \qquad (6)$$

This frequency is a maximum when R_j equals R_{min}. The self-resonant frequency is significant because at operating frequencies below f_{xo}, the reactance of the diode is capacitive; above self-resonance, it is inductive.

Circuit Behaviour

Further analysis of the small-signal equivalent circuit of Fig. 11 also provides useful application information. The operation of a tunnel diode as a stable amplifier, sinusoidal oscillator, relaxation oscillator, or switch is determined by the values of R_s, R, C_j, L_s, and R_L, where R is the magnitude of the negative resistance (usually is minimum value, R_{min}) and R_L is the external resistance. The conditions which must be satisfied for the different operating modes are shown in Fig. 12. This chart is plotted in terms of the following parameters:

$$\propto \equiv \frac{R_s + R_L}{R} \qquad (7)$$

$$\beta \equiv \frac{(R_s + R_L)\ RC_j}{L_s} \qquad (8)$$

The value of $\propto$ determines whether or not the diode operates as a switch. When $\propto$ is greater than 1, the load line can intersect the current-voltage characteristic at two stable points, as shown in Fig. 13. The diode then acts as a bistable switch. When $\propto$ is less than 1, the diode can be used as an oscillator or amplifier, depending on the values of both $\propto$ and β. Because this
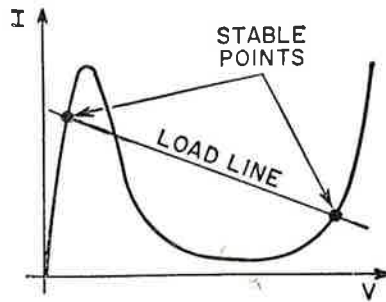

Fig. 13—Tunnel diode load-line chart.

chart is based on a small-signal analysis, the relationships between R_s, R, L_s and C do not apply for the steady-state case of an oscillator. Under steady-state conditions, however, the negative resistance has an effective value, R', such that $\beta = 1$. For this condition, the actual frequency f of a sinusoidal oscillator becomes

$$f = \frac{1}{2\pi R' C_j} \sqrt{\frac{1}{(R_s + R_L)} - \frac{1}{(R'C_j)^2}} \qquad (9)$$

and because $\beta = 1$, this equation may be simplified as follows:

$$f = \frac{1}{2\pi} \sqrt{\frac{1}{L_s C_j} - \frac{R_s{}^2}{L_s{}^2}} \qquad (10)$$

Temperature Variation of Parameters

To some extent, all electrical parameters of the tunnel diode are affected by temperature variations. In general, the tunnelling region of the current-voltage characteristic curve is least affected; the greatest temperature variations occur in the injection region.

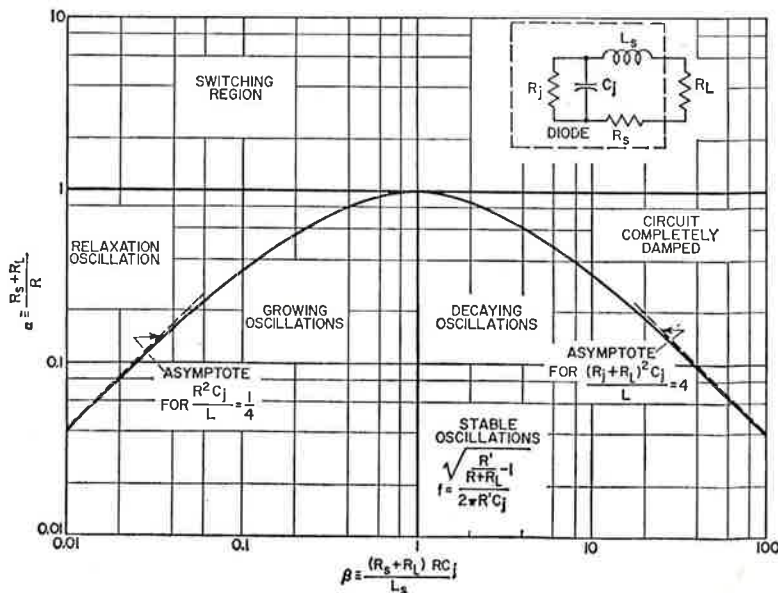The temperature dependence of the peak current of tunnel diodes is a function of the carrier

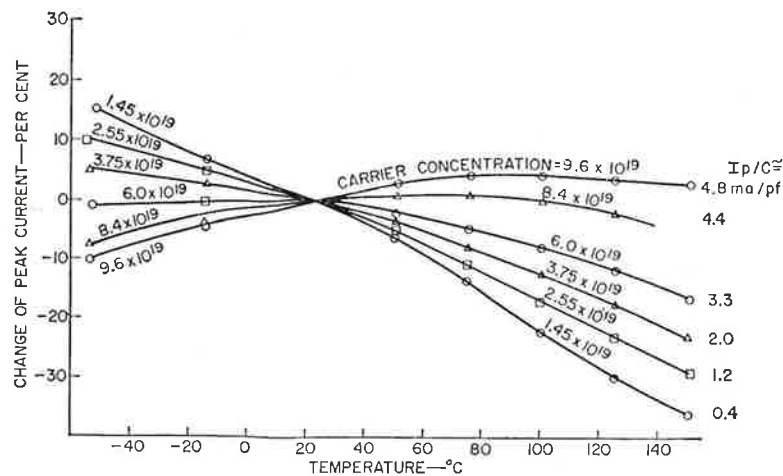Fig. 12—Tunnel diode performance chart.

Fig. 14—Percentage change of peak current as a function of temperature for different values of carrier concentration and speed index.

concentration of the crystal used.[1] Fig. 14 shows peak current of a germanium tunnel diode as a function of temperature for different values of p-region carrier concentration. As the doping density is increased, the temperature coefficient changes from negative to slightly positive. Thus, tunnel diodes having excellent peak current-vs.-temperature characteristics can be produced by proper choice of carrier concentration.

Because the diode speed index (I_P/C_j) is a sensitive function of carrier concentration, it is not always possible to achieve a desired temperature response consistent with a speed index required for a given application. Fortunately, the temperature coefficient of high-speed germanium tunnel diodes is small near room temperature. Fig. 14 also shows the diode speed index corresponding to each value of carrier concentration. Fig. 15 shows typical variations in peak current with temperature for germanium type IN3855.

Peak voltage is not greatly affected by temperature variations. This parameter has a small negative coefficient, and is slightly dependent on the peak current of the diode. For example, the peak voltage of a 50-milliampere germanium diode having a carrier concentration of about 7.0×10^{19} per cubic centimetre changes by approximately 2 millivolts from 0 to 100 degrees Centigrade, or about 20 microvolts per degree. For a five-milliampere diode having an average carrier concentration of 3.5×10^{19} per cubic centimetre, the peak voltage changes approximately 4 millivolts from 0 to 100 degrees Centigrade, or about 40 microvolts per degree. The slight dependence on peak current may result from the fact that the measured peak voltage V_P is composed of two components, as follows:

$$V_P = V_{Po} + I_P R_s \qquad (11)$$

where V_{Po} is the inherent peak voltage of the

diode and $I_P R_s$ is the voltage drop across the series resistance. Because peak current is temperature-dependent, as discussed previously, temperature variations of the peak current also affect the peak voltage. Fig. 16 shows typical variations of peak voltage as a function of temperature.

Valley current has a higher temperature coefficient than other tunnel-diode parameters, and the coefficient itself increases with temperature. For example, the valley current of several five-milliampere germanium tunnel diodes doubles in value from —35 to 100 degrees Centigrade, as shown in Fig. 17. This parameter is only slightly dependent on carrier concentration.

As shown in Fig. 18, the valley voltage has an approximately linear negative temperature coefficient which ranges from —0.8 to —0.9 millivolts per degree Centigrade.

The forward voltage region also exhibits a negative temperature coefficient. The projected peak voltage V_{PP} has a linear negative temperature coefficient of approximately 1.0 millivolt per degree Centigrade, as shown in Fig. 19. This parameter is slightly dependent on peak current and doping density. For example, typical 50-milliampere germanium diodes may have a tem-
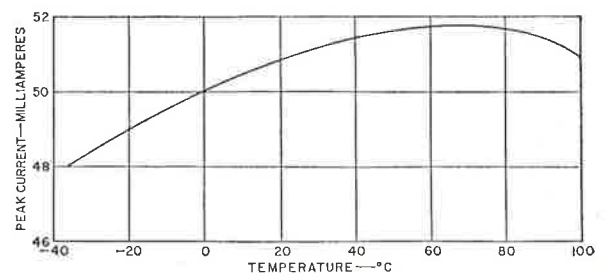

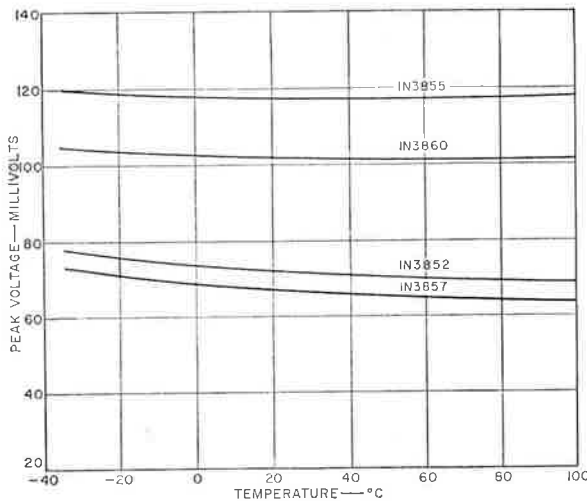Fig. 15—Temperature coefficient of tunnel diode peak current.

Fig. 16—Temperature coefficient of tunnel diode peak voltage.

perature coefficient for forward voltages as low as —0.9 millivolt per degree Centigrade; a five-milliampere unit may have a typical coefficient of —1.1 millivolts per degree Centigrade. This variation results partly from the method by which the forward-voltage point is defined and measured. Because V_{PP} is measured at a current equal to the peak current, it is measured at correspondingly lower current levels when the peak current decreases with increasing temperature. (For purposes of comparison, the temperature coefficient of conventional germanium diodes is in the area of 2.5 millivolts per degree Centigrade; this rating is much poorer than that of tunnel diodes.)

Because such devices as tunnel rectifiers are operated in the reverse-bias region, it is also
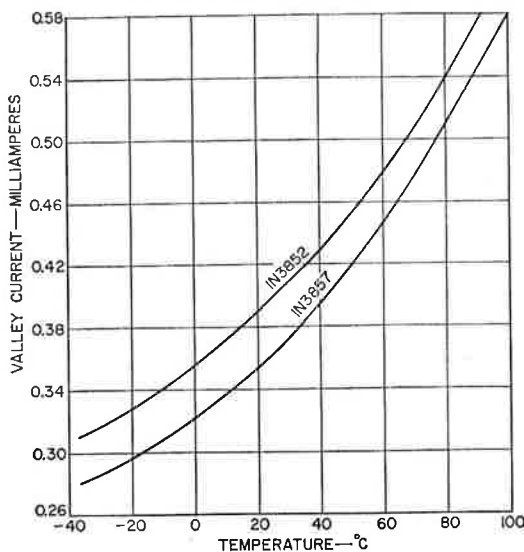

Fig. 17—Temperature coefficient of valley current.

important to consider the temperature coefficient of the reverse characteristic. Fig. 20 shows the per cent change in reverse voltage with a constant reverse-current bias. As shown, the total change over the entire temperature range is less than one per cent.

Life Stability of Ge Types

Accelerated life tests at RCA have shown no inherent failure mechanisms for germanium tunnel diodes. Figs. 21 and 22 show results of long-range tests on type IN3129 diodes. The only deviations in characteristics were slight increases in valley current and slight decreases in valley voltage. In general, the results of shelf-life tests at 100 degrees Centigrade were also very favourable, as were operating life tests within reasonable dissipation limits.
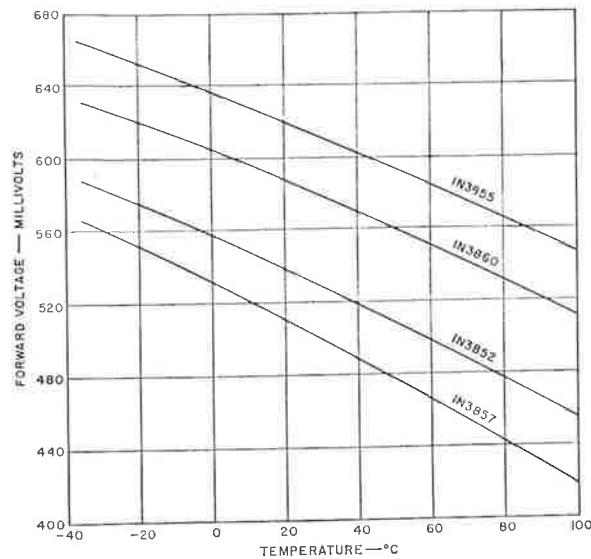

Fig. 18—Temperature coefficient of tunnel diode valley voltage.

An accelerated life test was conducted to determine the long-term stability of the peak current of germanium tunnel diodes. In this test, three types of diodes were operated at 25 degrees Centigrade, and at average currents several times the specified peak currents of 50, 25 and 5 milliamperes, respectively. Equipment having an accuracy better than 0.25 per cent was used for measuring peak and valley currents. Voltage measurements were accurate to within one per cent.

After 5000 hours of testing, no open or short circuits occurred in any of the units. All five-milliampere diodes, as well as 80 per cent of the 25- and 50-milliampere units, had a peak-current stability of ± 1 per cent or better. None of the units changed more than ± 1.5 per cent in peak current. Average peak-current changes

for the five-, 25-, and 50-milliampere types were 0.13 per cent, 0.56 per cent, and 0.70 per cent, respectively. Changes in peak voltage averaged less than one millivolt.

All units that had an initial peak-to-valley current ratio greater than 10:1 remained at that ratio after 5000 hours of testing. However, the valley current for a few of the 25-milliampere diodes having an initial ratio of less than 10:1 changed significantly. The average decrease in current ratio for the 50-milliampere and 25-milliampere diodes was 0.9 (for example, from 9.8:1 to 8.9:1). The average ratio for the five-milliampere diodes decreased by approximately 0.5.

Valley-voltage and forward-voltage changes were found to be inversely proportional to the valley-current changes; however, the percentage change in valley and forward voltage was not as great as that of the valley current.
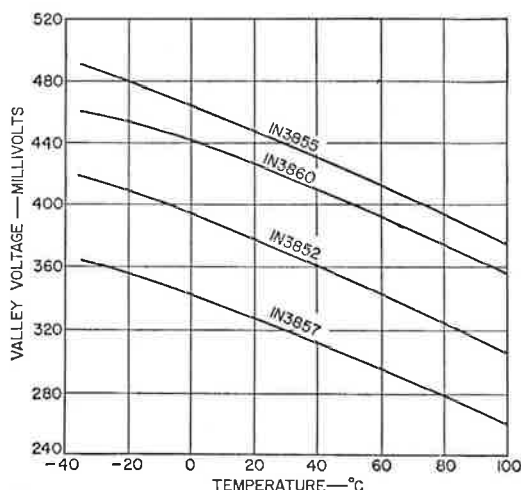

Fig. 19—Temperature coefficient of tunnel diode projected peak voltage.

In another precision life test, high-speed units (50 milliamperes, seven picofarads) operated at accelerated dc conditions (average current several times the peak current) showed somewhat greater changes in peak and valley currents. After 4000 hours, some units exhibited peak-current degradations up to three per cent. In this life test, the power level used was about five times that normally encountered in typical logic circuits such as monostable amplifiers or gates.

Life Stability of GaAs Types

As previously mentioned, gallium arsenide tunnel diodes offer several advantages over germanium devices. For example, they provide a voltage swing twice the size of that available with germanium. In addition, because the power output at a fixed impedance level varies as the square of the voltage swing, the power output of gallium
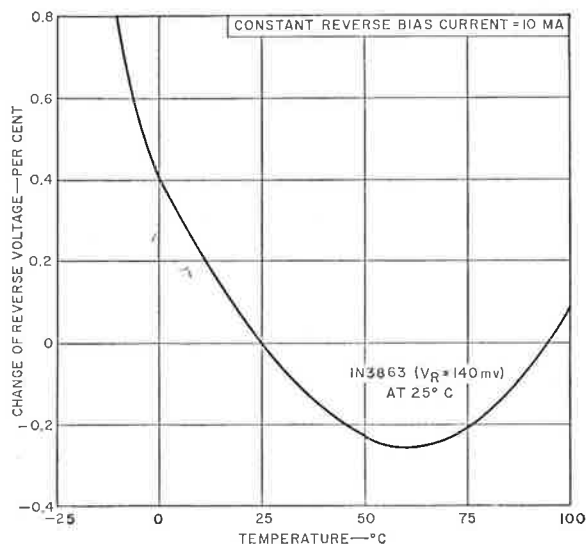

Fig. 20—Temperature coefficient of tunnel diode reverse voltage.

arsenide devices is about four times that of germanium tunnel diodes having the same negative resistance. When gallium arsenide diodes are operated at high current levels in the forward-injection region, however, serious degradation of the peak current can occur if certain operating limitations are not considered. This degradation, which is believed to be the result of the energy associated with the recombination of injected minority carriers,[2-4] is characterized by decreases in peak current, decreases (or increases) in valley current, and small changes in capacitance and voltage.

No degradation has been observed during operation of gallium arsenide diodes in the reverse region or in the tunnelling region. For example, 5-milliampere units have been operated at a reverse current of 50 milliamperes with no noticeable degradation after 2000 hours. Operation in the negative-resistance region (as an oscillator) produces no degradation even at temperatures up to 150 degrees Centigrade. When the diode is operated as a relaxation oscillator and the signal
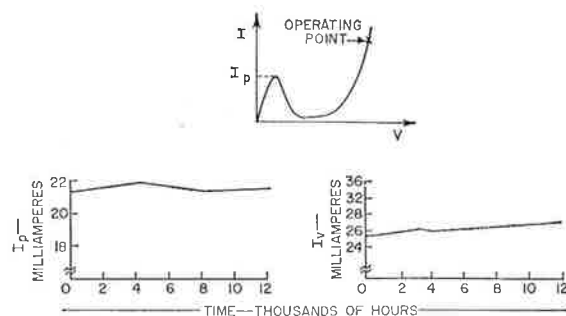

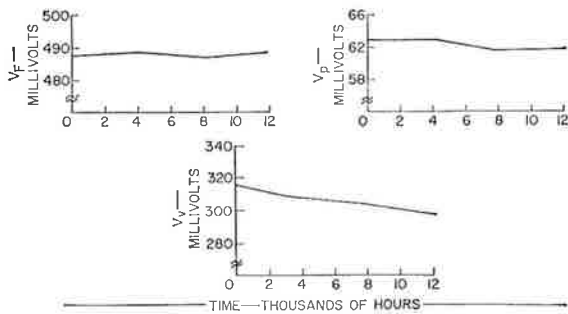**Fig. 21—High-stress life test results for I_p and I_v of a pre-aged type 1N3129.**

Fig. 22—High-stress life test results for V_f, V_p and V_v of a pre-aged type 1N3129.

swing is quite large, however, the resultant excursions into the forward region may result in degradation unless the precautions described below are observed.

The degradation rate depends on the peak-current-to-capacitance ratio (I_P/C_j) and the forward voltage, as well as on the forward current. For example, 50-milliampere units were operated at three different current levels (10, 25, and 50 milliamperes) in the forward region. After 800 hours, the units operated at ten milliamperes showed no degradation; the units operated at 25 milliamperes showed degradation of one to five per cent, and the units operated at 50 milliamperes showed degradation of 5 to 25 per cent. In addition, units having the highest speed ratio showed the greatest degradation.

On the basis of extensive life data[5], a limiting condition for safe dc operation of diffused gallium arsenide tunnel diodes at room temperature has been empirically established. This condition is given by

$$\frac{I}{C_j} \leqq 0.5 \text{ ma/pf} \qquad (12)$$

where I is the average current in milliamperes and C_j is the junction capacitance in picofarads. When the above condition is satisfied, degradation is negligible for any given operating conditions beyond the valley voltage. Fig. 23 shows the results of testing of two tunnel diodes under these conditions. These tests were still in progress during the publication of this manual.

The limiting condition is applicable for both tunnel rectifiers and tunnel diodes. In addition, it applies to high-current diodes which are operated at less than the peak current in the forward region, as well as to low-current units operated at currents greater than the peak current.

SAMPLE No.	CRITICAL I_p (ma)	DOSE NECESSARY TO CHANGE I_p BY 5% (nvt × 10^{17})
1	87·0	1·63
2	79·0	1·35
3	38·9	1·52
4	36·6	1·20
5	26·2	1·52
6	16·4	2·89
7	4·0	2·75
8	4·3	2·75
9	55·0	1·41
10	53·0	0·76

Table 3—Radiation effects on peak current. Samples 1 to 6 inclusive are germanium types, and samples 7 to 10 inclusive are gallium arsenide types.

Radiation Effects

Recent tests have shown that tunnel diodes are several orders of magnitude more resistant to nuclear radiation than bipolar transistors. The principal reason for this high resistance to radiation damage is that the tunnel diode is a majority-carrier device. As a result, its electrical characteristics are virtually independent of minority-carrier life times. The operation of the bipolar transistor, on the other hand, depends on minority-carrier life time. The high-energy par-
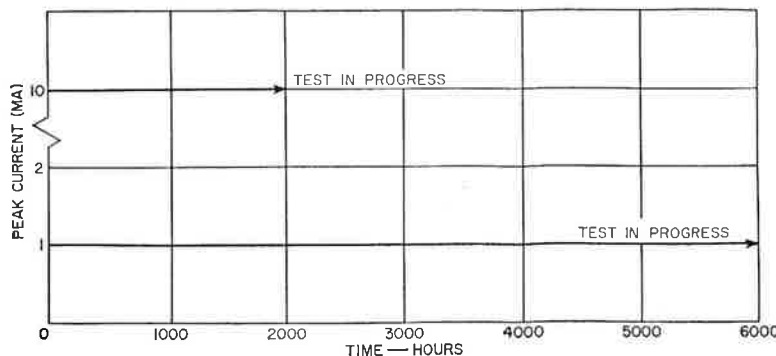

Fig. 23—Typical life stability of gallium arsenide tunnel diodes.

SAMPLE No.	INITIAL I_p/I_v	DOSE NECESSARY TO REDUCE I_p/I_v (nvt $\times$ 10^{15})		
		0·9 I_p/I_v	0·75 I_p/I_v	0·5 I_p/I_v
1	6·4	6·05	22·2	80
2	6·6	7·0	34·0	150
3	7·8	4·1	22·0	57
4	6·8	4·1	23·0	100
5	6·1	4·1	35·0	126
6	3·6	8·5	34·0	165
7	6·8	5·4	18·0	17
8	6·0	5·4	18·0	65
9	23·9	2·7	13·0	37
10	19·6	1·1	9·0	38

Table 2—Radiation effects on the peak-to-valley ratio. Samples 1 to 6 inclusive are germanium devices, and samples 7 to 10 inclusive are gallium arsenide types.

ticles introduced by radiation can seriously reduce life times of minority carriers and thus degrade transistor performance.

In a series of tests, ten tunnel diodes (six germanium and four gallium arsenide) were subjected to heavy doses of radiation. The data from these tests show that the parameter most affected by radiation is the valley current, which increased significantly at dosage levels of 10^{17} nvt (neutrons per square centimeter). This rise in valley current is believed to be a result of the additional energy states within the bandgap of the device which are formed by the neutron bombardment. The current increase is linearly dependent on the total integrated flux. As shown in Table 2, the increased valley current reduces the peak-to-valley current ratio as radiation is increased. The tests also indicated that peak current is relatively unaffected by radiation, as shown in Table 3.

References

1. A. Blicher, R. Glicksman, R. M. Minton, "Temperature Dependence of the Peak Current of Germanium Tunnel Diodes", *Proc. IRE, 49,* 9, p. 1428, Sept., 1961.
2. R. D. Gold and L. R. Weisberg, "The Degradation of GaAs Tunnel Diodes", *IRE Tran. on Elect. Devices, ED-8,* August, 1961.
3. R. L. Longini, "Rapid Zinc Diffusion in Gallium Arsenide", *Solid State Electronics,* 5, p. 127, May-June, 1962.
4. H. J. Henkel, "Aging Phenomena in Gallium Arsenide Tunnel Diodes", *Z fur Naturf., 17a,* p. 358 (1962).
5. A. Pikor, G. Elie, R. Glicksman, "Some Factors Affecting the Degradation of GaAs Tunnel Diodes",

PHASE AND FREQUENCY
— AND THE OSCILLOSCOPE

The cathode ray oscilloscope offers us one of the simplest and at the same time one of the most accurate methods of comparing frequencies and phase differences. The technique involves the study of "Lissajou" figures, which are produced on the CRO when data applied to the X and Y deflection facilities have a relationship, either in frequency or phase, or sometimes in both.

A "Lissajou" figure results from the simultaneous deflection of the CRO spot in both the X and Y axes. We know that when two deflection forces acting at right angles are applied to a body, the vector sum of the two forces produces a force and a movement of the body in a third direction. The speed and direction of movement of the body depend upon the instantaneous magnitude of the two deflecting forces. In this case the two deflecting forces are X and Y voltages in the CRO, and they move the spot to trace the pattern on the face of the tube.

Once the principle of operation is understood, a new and versatile tool is available to us. The shapes of the figures traced out on the face of the CRO tube can be interpreted into useful data. In theory, there is an endless variety of "Lissajou" figures which can be formed, but in practice the ones that we use are generally restricted to those in which the relationship between the X and Y voltages is not greater than about 10 : 1.

Phase Measurement

Fig. 1 shows an instantaneous condition similar to that just described, in which two forces at right angles, OB, OA, are acting upon a body

at O. The instantaneous vector sum OC represents the speed and direction of movement of the body, which in this argument is the CRO spot.

In practice we are interested in alternating voltages or deflection forces, which may vary either constantly or periodically with respect to each other in frequency, amplitude or phase, or in all three together. As a starting point, however, let us consider two alternating voltages in which the frequency, phase and amplitudes are the same. If these two voltages are applied to the X and Y deflection plates of the CRO, then, using our simple mechanical laws, we can determine graphically the movement of the spot, and the shape of the trace which will result on the face of the tube.
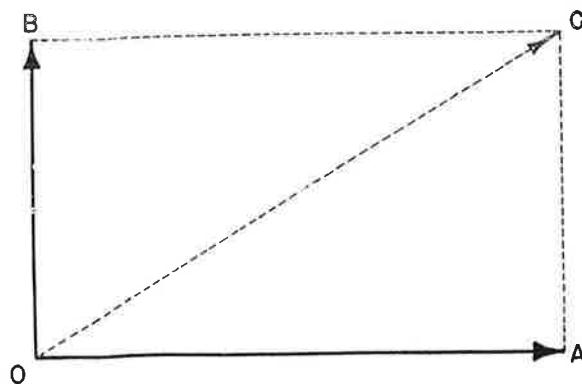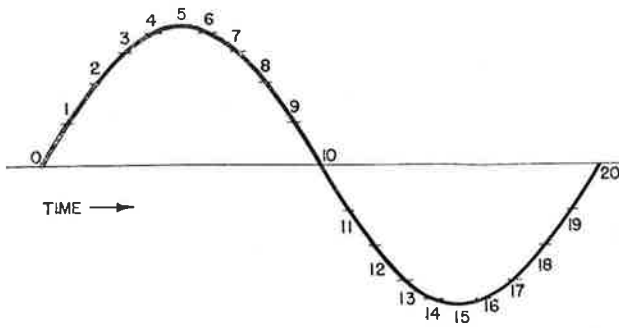

Fig. 1

Fig. 2

The graphical construction is shown in Fig. 2, in which the two sine waves are seen in their correct relationship, and in which the resultant trace on the tube is also shown. Arbitrary time intervals are shown on the two waves, and on the resultant, which is formed by projecting the time points until they intersect.

Certain interesting and vital information is immediately available to us. Firstly, two voltages having the same phase will produce a straight line on the CRO. Secondly, if the two voltages are of the same amplitude, the straight line will intersect the vertical and horizontal axes at an angle of 45 degrees. Before going further, it will be interesting for readers who may not yet have met this technique to reflect on, and possibly plot, two further conditions. One of these would be to assume a 180-degree phase shift in both of the sine waves, and see what happens, whilst the other would be to study the effect when the two voltages are still of the same phase, but vary in amplitude with respect to each other.

The next thing to be considered is a phase difference between the two input sine waves. A phase difference of 180 degrees between the two voltages will, following what has already been said, produce zero deflection of the spot, because the resultant force will always be zero. The next step, therefore, is to consider a phase difference of 90 (or 270) degrees. This condition is shown in Fig. 3, where the resultant trace is also shown.

The resultant trace is plotted in the same way as previously described, and may be replotted by the reader if necessary, in order to prove the construction. We see another most interesting fact, that the trace is a circle if the voltages are equal and phased 90 (or 270) degrees apart. If the phase difference remains the same, but the relative amplitudes of the two signals are changed, the trace becomes an ellipse. The shape of the
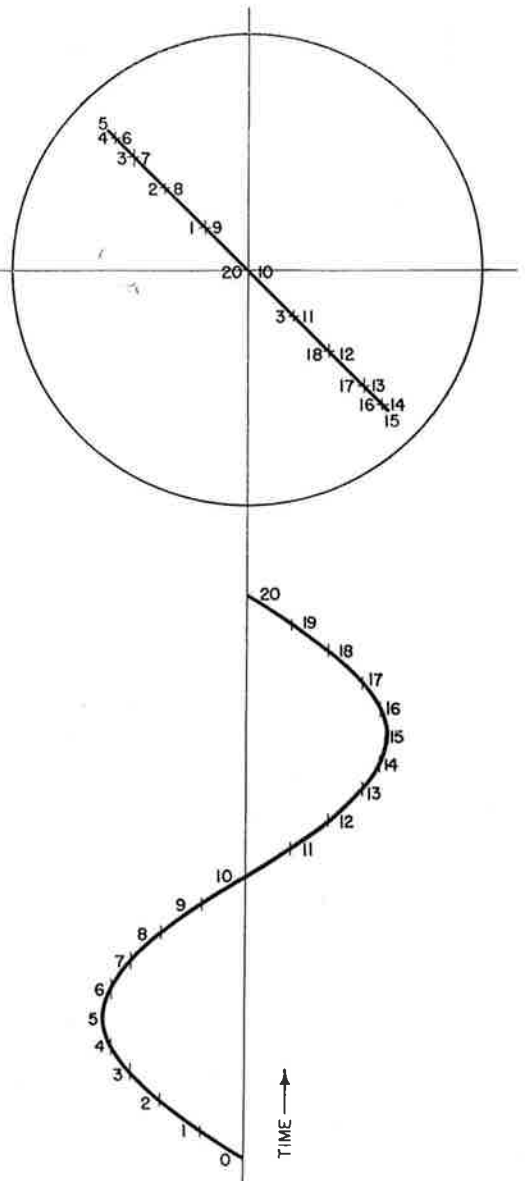
ellipse is determined by the relative amplitudes of the two voltages, and the long axis of the ellipse will lie along either the vertical or horizontal axis of the CRO, depending on which of the two voltages is the higher.

It is now possible to construct graphically the resultant of other phase differences, and a selection is shown in Fig. 4. The zero phase difference and 90 and 270-degree phase difference conditions are already familiar. Other conditions can be arrived at quite readily, either by plotting or by deduction.

It will be seen that this technique may be used to compare and measure phase differences. Because the CRO will handle frequencies cover-
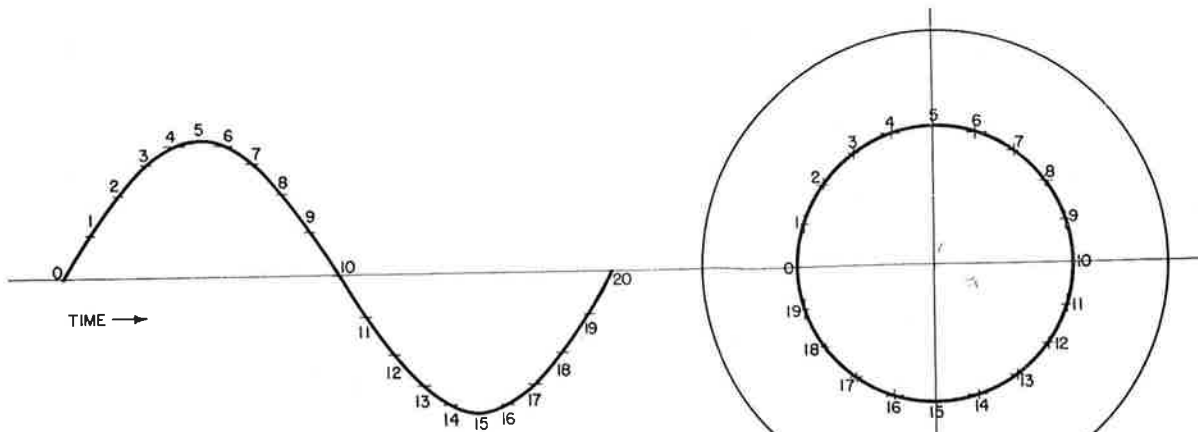
Fig. 3

ing a wide spectrum, we can use this device to make measurements up to quite high frequencies. A high degree of accuracy can be achieved by this method in the measurement of phase differences. For sine wave inputs, which are those with which we are most concerned, angular phase difference may be calculated from the trace on the CRO, following the diagram shown in Fig. 5, and using the expression:

$$\frac{OC}{OD} = \sin \beta \text{ or } \frac{AB}{4 V_1 V_2} = \sin \beta,$$

where β is the phase difference in angular degrees, V_1 is the zero-to-peak value of the horizontal voltage, and V_2 is the zero-to-peak value of the vertical voltage.

It can be seen that there will be more than one solution. The selection of the correct answer will depend upon the notation of the quadrant from the orientation of the major axis of the ellipse and the direction of spot motion. Doubt can usually be resolved by shifting one of the voltage inputs slightly in phase in a known direction and noting the result on the shape of the pattern.

Note that the expressions given here for measurement of phase shift graphically must be used with care if the two input voltages are applied to the deflection plates through amplifiers. Unless the phase distortion characteristics of the X and Y amplifiers are identical at the operating frequency, or the differences are known so that a correction can be applied, error may result.

Frequency Measurement

In the discussion of phase measurement, the simplest type of "Lissajou" figures, the circle and the related ellipse were the only ones used. It is now necessary to consider what happens when the frequencies of the input voltages are changed
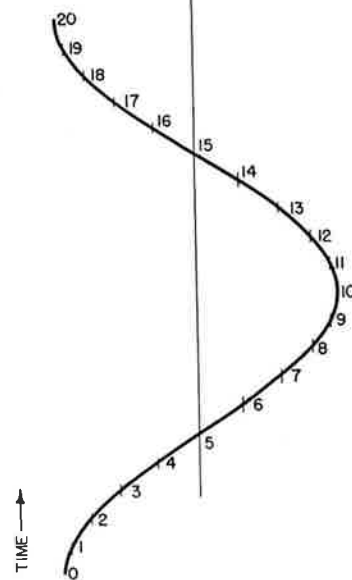
with respect to each other, and how the types of pattern obtained may be used.

If a vertical deflection signal is applied so that its frequency is exactly an integral number of times that of the horizontal deflection signal, a stationary pattern will be obtained on the CRO. A typical pattern is shown in Fig. 6, which represents a vertical-to-horizontal frequency ratio of 3 : 1. Inspection will show this to be true. The horizontal deflection is applied from left to right and back to the start in a time corresponding to one cycle. In this time, as the diagram shows, the vertical deflection element has gone through three complete cycles, so that the vertical frequency must be three times that of the horizontal frequency.
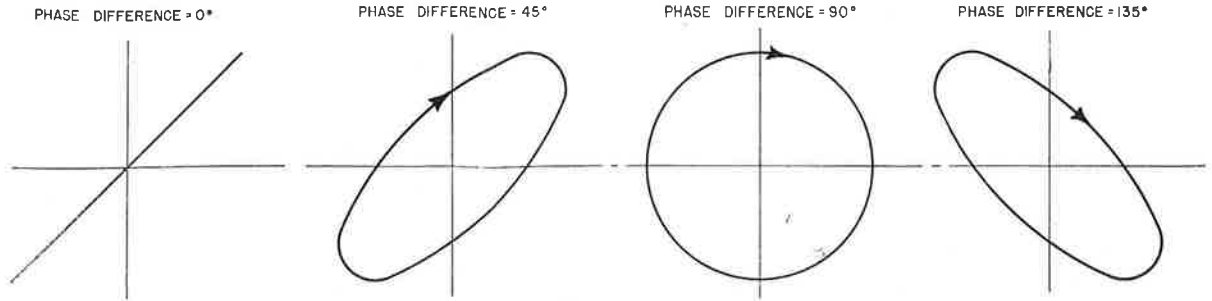
PHASE DIFFERENCE = 0°   PHASE DIFFERENCE = 45°   PHASE DIFFERENCE = 90°   PHASE DIFFERENCE = 135°

Fig. 4

If the frequency factor is not an integer, the pattern will appear to rotate. It should be noted that for a given frequency ratio, a number of patterns can be obtained, such as a pattern representing a ratio of 6 : 2 or 9 : 3. These patterns will of course provide exactly the same information, but for the sake of simplicity and accuracy we usually prefer to use the lowest possible ratio display.

A very high accuracy of measurement can be achieved by this method, and it will readily be seen that if a calibrated frequency standard is attached to the X deflection terminals and unknown frequencies are fed into the Y terminals, the unknowns can be determined by adjusting the standard for a stationary figure with a simple ratio, and then doing a simple bit of arithmetic.

A selection of "Lissajou" figures obtained in frequency measurement work is shown in Fig. 7, together with the frequency ratios represented. In some cases the right-to-left portion of the trace is shown dotted to assist the eye in following what takes place. Where the pattern becomes more complex, and the frequency ratio is not obvious

from inspection, it is necessary to imagine a rectangle enclosing the pattern. We then compare the number of points tangent to the horizontal sides with the number of tangent points on the vertical sides. This will give us the required ratio.
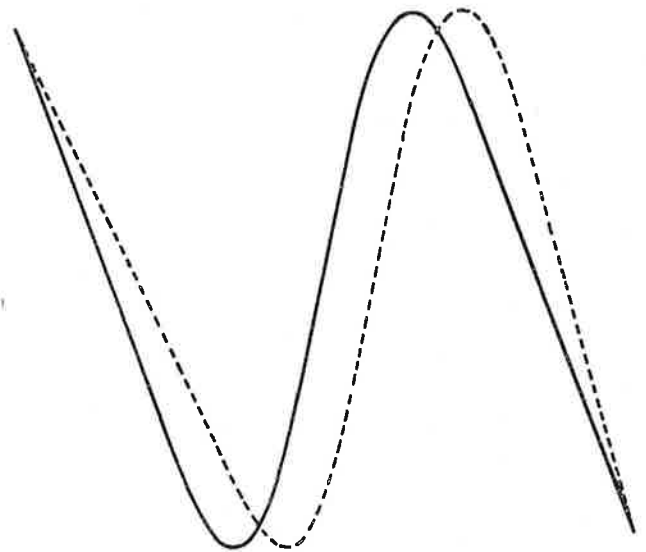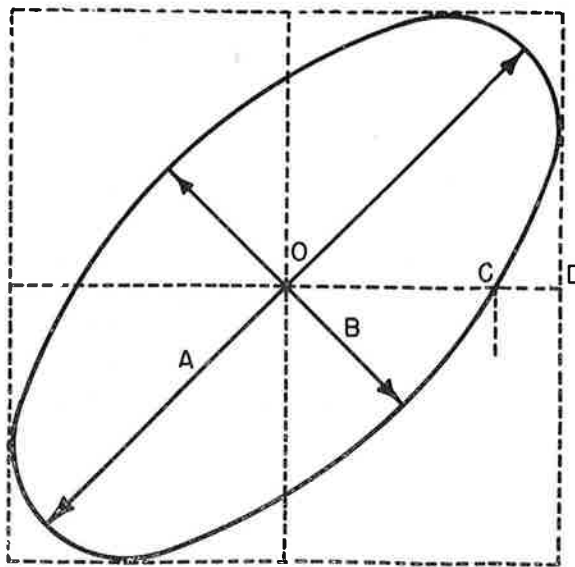

Fig. 6

Another method of evaluating a more difficult pattern is to count the number of peaks along the top edge of the imaginary rectangle and divide by the maximum number of intersections in the figure along any vertical line. In general, the higher the frequency ratio, the more difficult the analysis of the results.

For ratios higher than can be conveniently used in the method just described, two alternative methods are available. In the first of these, the lower of the two frequencies is fed through a phase splitting network to provide two components with a 90-degree phase difference; these components are then used to provide a circular sweep on the CRO. The higher frequency is then used to modulate the second anode of the CRO tube, producing a "gear-wheel" display similar to that shown in Fig. 8. This figure, incidentally,
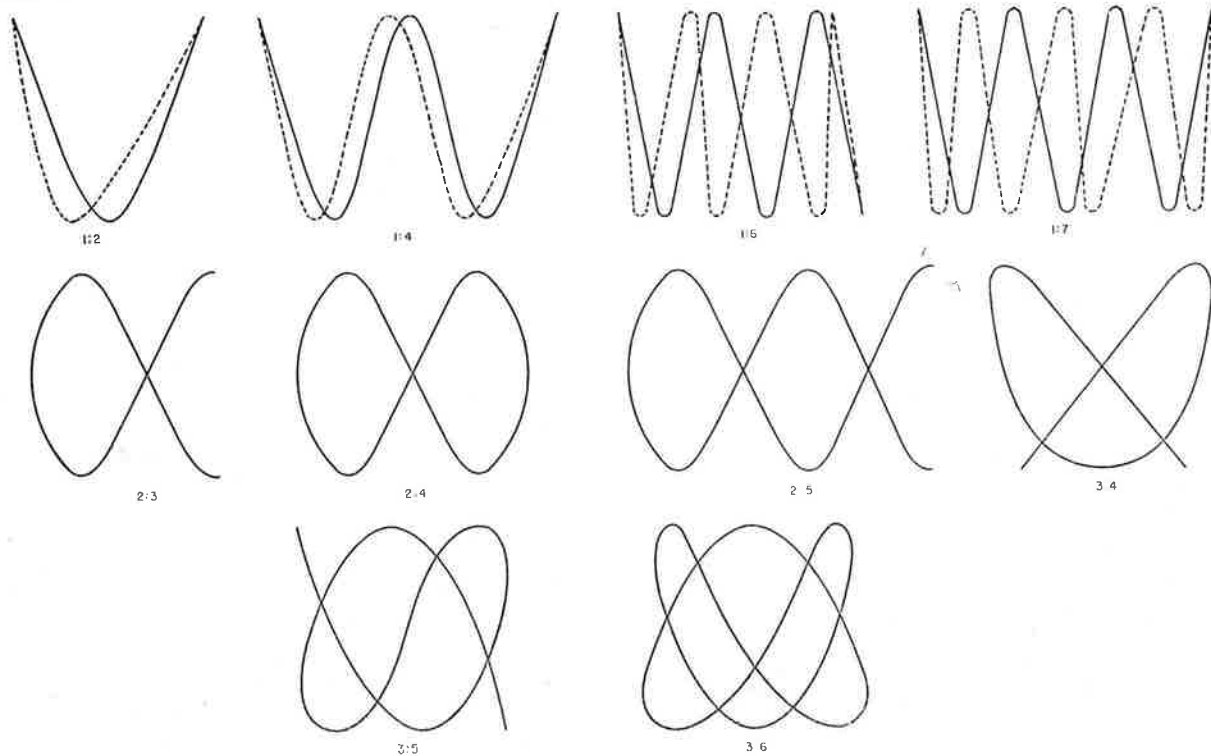

Fig. 5

Fig. 7

represents a ratio of 12 : 1, the ratio being determined simply by counting the number of gear teeth.

The second method of dealing with large ratios is similar to that just described, except that the higher frequency is used to modulate the grid of the CRO tube instead of the second anode.
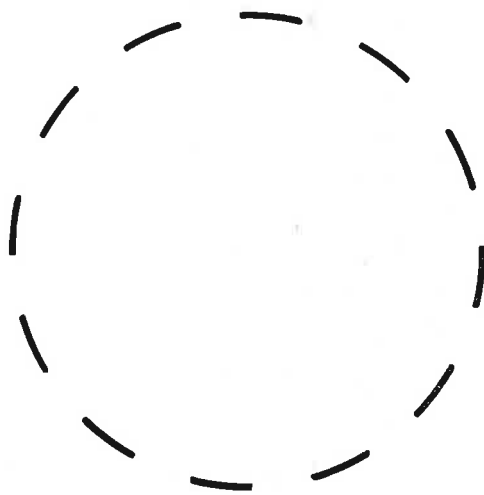
In this case a dotted circular display is observed, as shown in Fig. 9, which also represents a ratio of 12 : 1. Here the ratio is determined by counting the number of dots in the circumference of the circle.

In general, only very simple types of CRO are needed to make phase and frequency compari-
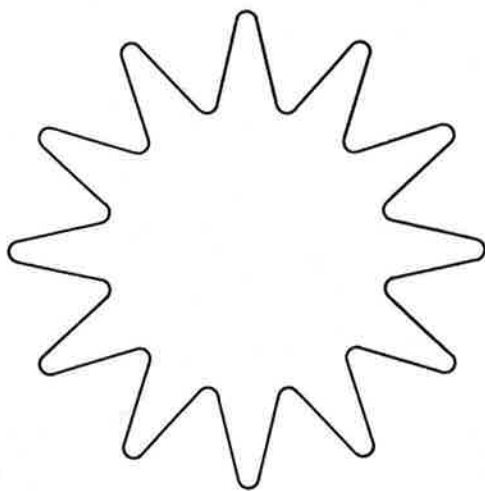

12:1

Fig. 8

12:1

Fig. 9

sons of the type described. It will be noted that only normal CRO's are used in these examples, although for specialised work there are other types of display which could also be used. For example, a J-scan, circular time base with central radial deflecting electrode, would be very suitable for the "gear-wheel" method.

These simple techniques allow us to measure frequency and phase to a high order of accuracy. To quote only one example, a simple set-up allows us to measure phase shift in an amplifier at various frequencies, an important point where negative feedback is to be applied. It has truly been said that even the simplest CRO is one of the most useful and versatile tools we have.
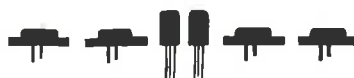
OPTICAL MASERS

(Continued from page 174)

Another class of applications is also dependent on the spatial coherence of the optical maser. The energy from a 1-watt maser could be focused to a spot 10^{-4} centimeters in diameter, producing at the focal point power densities of 100 mega-watts/cm². The optical-frequency electric fields associated with such power densities are of the order of 30,000 volts cm. It is clear that such fields and power densities can produce chemical and physical reactions in matter under conditions that cannot be duplicated by any other technique. Thus, optical masers may play an important role in molecular electronics technology and micro-chemistry.

It is difficult to foresee all the possible applications of a device with such radically different characteristics at such an early state of its development; but it can be seen that optical masers may find uses in the areas of activity in which RCA is engaged.

BIBLIOGRAPHY

1. R. H. Dicke; *U.S. Patent 2, 851, 652;* filed May 21, 1956; issued Sept. 9, 1958.
2. J. M. Brumbaugh, D. Karlsons, L. C. Morris, and Dr. H. J. Gerritsen; "The Maser Microwave Amplification by Stimulated Emission of Radiation"; *RCA Engineer,* Vol. 6, No. 5, Feb.-Mar., 1961.
3. A. L. Schawlow and C. H. Townes; "Infrared and Optical Masers"; *Phys. Rev. 112,* 1940; 1958.
4. J. H. Sanders, "Optical Maser Design"; *Phys. Rev. Lett. 3,* 86; 1959.
5. A. Javan; "Possibility of Production of Negative Temperature in Gas Discharges"; *Phys. Rev. Lett. 3,* 87; 1959.
6. A. Javan, W. R. Bennett and D. R. Herriott; "Population Inversion and Continuous Optical Maser Oscillation in a Gas Discharge Containing a He-Ne Mixture"; *Phys. Rev. Lett. 6,* 106; 1961.
7. T. H. Maiman; "Stimulated Optical Radiation in Ruby"; *Nature 187,* 493; 1960.
8. P. P. Sorokin and M. J. Stevenson; "Stimulated Infrared Emission from Trivalent Uranium"; *Phys. Rev. Lett. 5,* 557; 1960.
9. P. P. Sorokin and M. J. Stevenson; "Solid State Optical Masers Using Divalent Samarium in Calcium Fluoride"; *IBM Journal of Research and Development, 5,* 56; 1961.
10. R. J. Collins, D. F. Nelson, A. L. Schawlow, W. Bond, C. G. B. Garrett and W. Kaiser; "Coherence, Narrowing, Directionality and Relaxation Oscillations in the Light Emission from Ruby"; *Phys. Rev. Lett. 5,* 303; 1960.

(With acknowledgements to RCA)